ISSN 0036-0236, Russian Journal of Inorganic Chemistry, 2006, Vol. 51, No. 1, pp. 118–125. © Pleiades Publishing, Inc., 2006.
Original Russian Text © L.P. Mezentseva, V.F. Popova, V.I. Al'myashev, N.A. Lomanova, V.L. Ugolkov, S.V. Beshta, V.B. Khabenskii, V.V. Gusarov, 2006, published in Zhurnal Neorganicheskoi Khimii, 2006, Vol. 51, No. 1, pp. 126–133.

PHYSICOCHEMICAL ANALYSIS OF INORGANIC SYSTEMS

Phase and Chemical Transformations in the SiO_2–$Fe_2O_3(Fe_3O_4)$ System at Various Oxygen Partial Pressures

L. P. Mezentseva*, V. F. Popova*, V. I. Al'myashev*, N. A. Lomanova*, V. L. Ugolkov*, S. V. Beshta, V. B. Khabenskii**, and V. V. Gusarov***

** Grebenshchikov Institute of Silicate Chemistry, Russian Academy of Sciences, ul. Odoevskogo 24/2, St. Petersburg, 199155 Russia*

*** Aleksandrov Research Technological Institute, Sosnovyi bor, Leningrad oblast, Russia*

Received February 8, 2005

Abstract—The SiO_2–$Fe_2O_3(F_3O_4)$ system has been studied in air, oxygen, and an inert atmosphere. The dissociation temperatures for iron oxides, the onset and full melting temperatures for coexisting phases, and the melt demixing temperatures have been determined as a function of the oxygen partial pressure. A scenario of the phase and chemical transformations in the title systems has been developed.

DOI: 10.1134/S0036023606010190

Oxide systems containing iron and silicon are of significance for metallurgy, for manufacturing of glass, ceramics, and refractories, and for other applications [1, 2]. Investigations into such systems have a long history [3–8].

The most comprehensive investigation of the phase and chemical transformations in the SiO_2–FeO–Fe_2O_3 ternary system was performed by Muan [7]. Muan also used data of other researchers [3, 9–11] to design a liquid–solid diagram. In particular, Muan [7] used the data on the FeO–Fe_2O_3 system from [9, 10] and on the SiO_2–FeO system from [11]. The boundary curve of the melt immiscibility region in the SiO_2–FeO–Fe_2O_3 system was drawn in accordance with the data borrowed from [5]. Most of Muan's investigations [7] were confined to the FeO–Fe_2SiO_4–Fe_3O_4 triangle and were carried out in a gas atmosphere of CO_2 and H_2 taken in different ratios in order to obtain different oxygen partial pressures. Only two compositions (one containing 12.3 wt % SiO_2 + 21.8 wt % FeO + 65.9 wt % Fe_2O_3 and the other containing 21.2 wt % SiO_2 + 23.2 wt % FeO + 55.6 wt % Fe_2O_3) were studied experimentally in air ($p_{O_2} \approx 0.21 \times 10^5$ Pa); two samples (one containing 12.9 wt % SiO_2 + 17.8 wt % FeO + 69.3 wt % Fe_2O_3 and the other containing 15.2 wt % SiO_2 + 17.7 wt % FeO + 67.1 wt % Fe_2O_3) were studied under an oxygen atmosphere ($p_{O_2} \approx 1.0 \times 10^5$ Pa). In addition, Muan [7] predicted a ternary eutectic to exist near the Fe_2O_3 corner with a provisional composition of 15 wt % SiO_2 + 16 wt % FeO + 69 wt % Fe_2O_3 and with a temperature of about 1455°C.

Extrapolating the data on the SiO_2–FeO–Fe_2O_3 system [7] and the hypothesized position of the immiscibility region in the SiO_2–Fe_2O_3 system [3, 12], Berezhnoi [13] designed a provisional phase diagram for the Fe_2O_3–SiO_2 system. Based on the data from [3, 7, 14], Fabrichnaya and Sundman [15] calculated the diagram for a section of the FeO–SiO_2–O_2 system.

Thus, the following issues remain to be studied systematically: the phase states of the SiO_2–Fe_3O_4–Fe_2O_3 system, specifically, in the region near the SiO_2–Fe_2O_3 side, and the phase and chemical transformations in the SiO_2–Fe_2O_3 system at oxygen partial pressures of $p_{O_2} \approx 0.21 \times 10^5$ and 1.0×10^5 Pa.

Therefore, the goal of this work was to experimentally determine the phase and chemical transformations in the SiO_2–$Fe_2O_3(Fe_3O_4)$ systems at different oxygen partial pressures in the gas atmosphere over the condensed phases.

EXPERIMENTAL

The starting chemicals used were analytical grade Fe_2O_3 (Specification TU 6-09-5346-87), 99.99% SiO_2 (rock crystal), and high-purity grade iron (Russian State Standard GOST 13610-79). Iron(III) oxide before blending was dried and calcined at 300°C, and silica, at 105°C for 3 h. Fe_3O_4 was prepared by annealing a $4Fe_2O_3$ + Fe blend at 1250°C for 1 h in corundum boats under flowing argon (high purity grade).

The phase composition of the samples was monitored using X-ray powder diffraction on a DRON-3 diffractometer using CoK_α radiation.

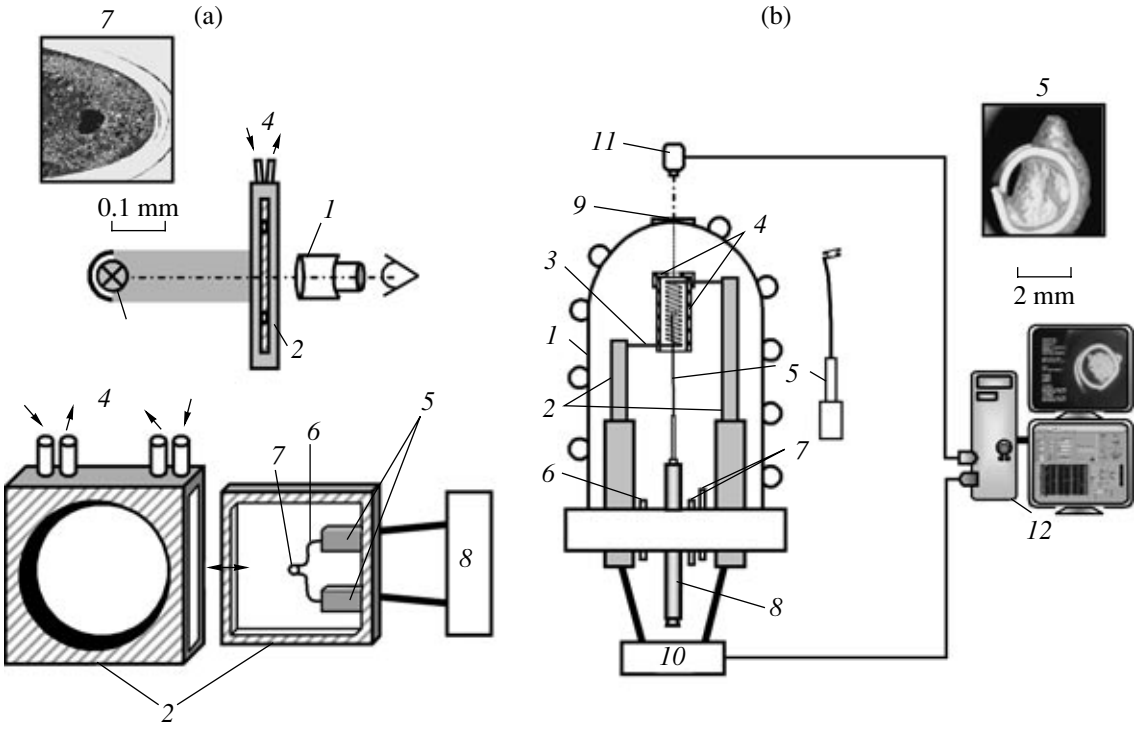

Fig. 1. Schematics of the VPA setups used. Panel (a): a high-temperature microscope: (*1*) long-focus microscope, (*2*) sealable heating chamber with silica glass windows and a container, (*3*) illumination system, (*4*) gas pipes, (*5*) silver electrodes, (*6*) looped iridium heater (sample holder), (*7*) a sample inside the looped iridium holder (a powder), and (*8*) power source. Panel (b): Galakhov's microfurnace: (*1*) water-cooled vacuum housing, (*2*) steel electrodes, (*3*) tungsten heating coil, (*4*) molybdenum shields, (*5*) sample holder (iridium or molybdenum), (*6*) pumping system, (*7*) gas feed system, (*8*) quenching device, (*9*) silica glass window, (*10*) controlled power source, (*11*) video camera, and (*12*) observation and monitoring system.

Thermal transformations in the systems were studied using complex thermal analysis (differential thermal analysis (DTA) plus thermogravimetry (TG)) on a Netzsch STA 429 thermal analyzer. In the DTA/TG experiments, platinum crucibles were used, the sample size was about 30 mg, the heating rate was 10 K/min, and the atmosphere was air, oxygen, or helium. The temperatures of thermal events were determined as the onset temperatures of relevant DTA peaks, which were found as the intersection of tangents to the baseline and the thermal curve.

The onset and full melting temperatures of the components of the system were also determined using visual polythermal analysis (VPA) on original design setups (a high-temperature microscope [16] (Fig. 1a) and Galakhov's modified microfurnace [17] (Fig. 1b)). The samples used in the VPA experiments were annealed at 1250°C in flowing argon and analyzed by X-ray powder diffraction.

The onset and full melting temperatures in the high-temperature microscope were determined on powdered samples weighing about 0.5 mg. The experiments were carried out in air ($p_{O_2} \approx 0.21 \times 10^5$ Pa) or in flowing oxygen ($p_{O_2} \approx 1.0 \times 10^5$ Pa). The ordinary error of the method for the specified temperatures is in the range ±(25–30)°C [16], but it can be higher because of the high viscosities of SiO_2-containing melts. The setup used allows employing high heating rates, which can result in extra overestimation of the temperatures to be determined. To avoid this, the heating was stepwise with arrests at intermediate steps. The onset melting temperature was determined as the onset of a visual displacement of the test substance to the top of the looped holder or to one of its sides, which resulted from the appearance of the first liquid portions. The full melting temperature was determined as the temperature at which the melt was spread over the looped holder *7* (Fig. 1a) or, for the samples with high silica concentrations (and with high melt viscosities), as the temperature at which the sample in the holder became transparent. The overall duration of the experiment was 30–60 s.

In the experiments in Galakhov's furnace, a sintered sample (7–8 mg) was mounted in holder *5*, which was placed in the isothermal zone of the microfurnace (Fig. 1b).

The working temperature range in the microfurnace was 900–2300°C. The temperature measurement error was about ±(25–30)°C [17]. The measurements were carried out in an inert atmosphere (high-purity helium) at an overall pressure in the system of about 0.25 ×

10^5 Pa. The design of the microfurnace allowed us to quench samples by dropping them, together with the holder, into the cold zone of the furnace. Melting of a sample was recorded with a digital video camera and analyzed frame by frame. The onset melting temperature was set equal to the temperature at which the acute angles of a chip of the sample started rounding during heating. The full melting temperature was set equal to the temperature at which the sample was spread over the surface of the holder. To avoid the interaction of the sample with the holder, the holder was made of iridium. The overall duration of an experiment was 30–120 s.

After quenching SiO_2–Fe_3O_4 samples, their microstructures were observed and elemental analysis was carried out using scanning electron microscopy (SEM) and energy-dispersive X-ray microanalysis (EDX) on an AVT-55 SEM equipped with a Link_AN_10000/S85 microprobe attachment.

To verify the measurement accuracy in Galakhov's microfurnace, the starting Fe_3O_4 was first melted (its melting point is 1597°C [18]). The melting was detected at 1614°C, in nice agreement (taking into account the error of the method) with the related literature for Fe_3O_4. To avoid overestimation of the critical temperatures, the heating rate in the region of these temperatures was 5 K/s.

RESULTS

The X-ray powder diffraction results showed that the SiO_2–Fe_2O_3 samples after the heat treatment at 1000 and 1100°C in air were mixtures of α-Fe_2O_3 and SiO_2 (quartz); at 1200 and 1300°C, they were mixtures of α-Fe_2O_3 and SiO_2 (quartz and cristobalite). By the way of example, Fig. 2 shows the X-ray diffraction patterns for a sample containing 94.8 mol % $FeO_{1.5}$ (for convenience of comparison, iron oxides hereafter appear as FeO_x: $FeO_{1.5}$ instead of Fe_2O_3, and $FeO_{1.33}$ instead of Fe_3O_4). The appearance of cristobalite (the high-temperature silica polymorph) in the X-ray diffraction pattern may be due to its stabilization as a result of dissolution of some iron oxide in an SiO_2-based phase.

X-ray diffraction shows Fe_3O_4 (as magnetite) and silica (as quartz and cristobalite) with trace tridymite in the SiO_2–Fe_3O_4 samples heat-treated in flowing argon at 1250°C (Fig. 2).

The DTA and TG data for the SiO_2–Fe_2O_3 samples in air and oxygen and for the SiO_2–Fe_3O_4 samples in argon are listed in Table 1. Figure 3 shows the TG and DTA curves (with peak resolution) for several SiO_2–Fe_2O_3 and SiO_2–Fe_3O_4 samples. The DTA curves recorded in air for the SiO_2–Fe_2O_3 samples each feature three endotherms with onset temperatures of about 1390, 1460, and 1470°C (Fig. 3a). The first endotherm

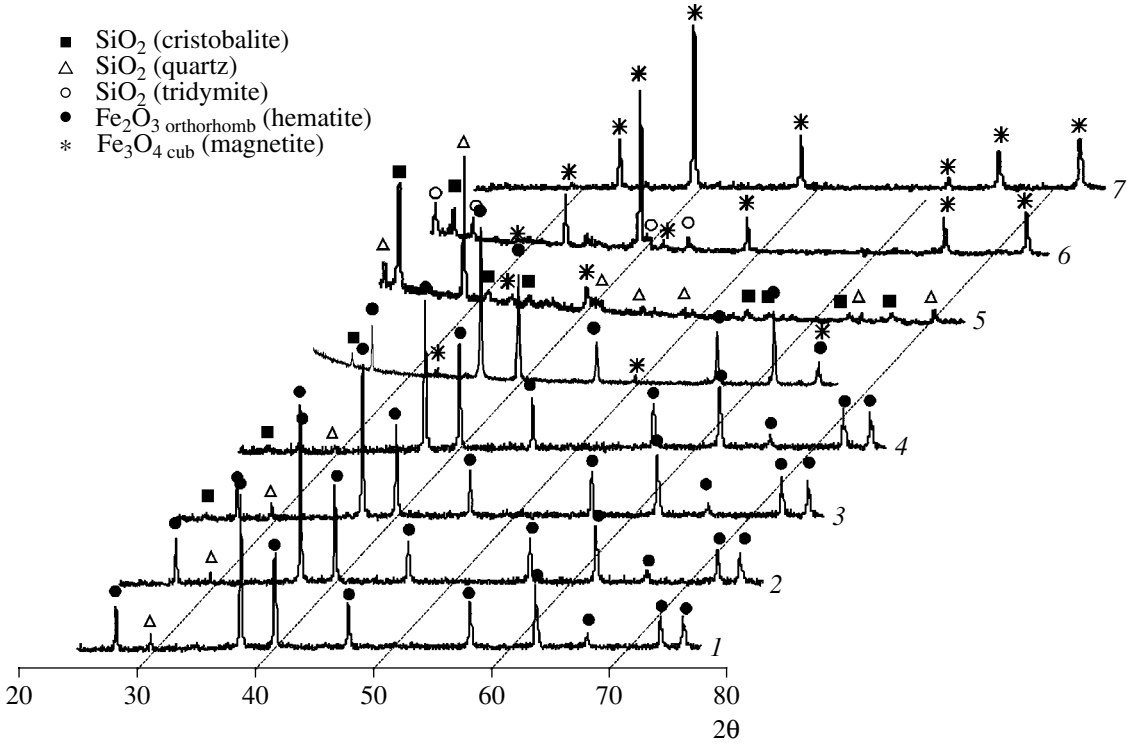

Fig. 2. (*1–5*) X-ray diffraction patterns for SiO_2–Fe_2O_3 samples containing 94.8 mol % FeO_x after heat treatment in air at (*1*) 1000, (*2*) 1100, (*3*) 1200, and (*4*) 1300°C and (*5*) after DTA in air up to 1400°C. (*6–8*) The same for SiO_2–Fe_3O_4 samples containing (*6*) 13.8, (*2*) 42.8, and (*8*) 96.2 mol % FeO_x after heat treatment in helium at 1300°C.

is accompanied by a significant weight loss, which then smoothly decreases to the second endotherm (Fig. 3a, Table 1). The third endotherm is superimposed on the second one and is almost unaccompanied by weight loss.

After the DTA/TG experiments carried out in air up to 1400°C, the phase composition of the samples was determined using X-ray powder diffraction. The X-ray diffraction pattern for the sample containing 94.8 mol % $FeO_{1.5}$ shows reflections of the Fe_3O_4 phase along with SiO_2 and Fe_2O_3 reflections (Fig. 2).

The DTA curves recorded in oxygen (Fig. 3b) show two overlapping endotherms with onsets at 1462 and 1473°C. The greatest weight loss is associated with the first endotherm.

For the SiO_2–Fe_3O_4 system, the DTA experiment was performed for the sample containing 42.8 mol % $FeO_{1.33}$ under helium and overall pressures of 1.0×10^5 and 1.2×10^5 Pa. The DTA curve shows two endotherms at 1424 and 1440°C; the former is accompanied by some weight loss (Fig. 3c, Table 1).

The onset and full melting temperatures of the SiO_2–Fe_2O_3 samples determined by VPA in the high-temperature microscope in air and oxygen are listed in Table 1. The determinations in air and oxygen gave identical values.

Analogous temperatures for the SiO_2–Fe_2O_3 samples as determined by VPA under argon in Galakhov's microfurnace are listed in Table 1.

The microstructure, phase composition, and chemical composition of the samples quenched from different temperatures in Galakhov's microfurnace were determined using SEM/EDX. Figure 4 exemplifies the microstructure of the samples prepared under the conditions that provided the melt-immiscibility onset (Fig. 4a) and the full separation of the melt into a silica-based phase and an iron oxide-based phase (Fig. 4b). The compositions of these phases are listed in Table 2.

DISCUSSION

The oxygen partial pressure affects the chemical processes that occur in the system until reaching the onset melting temperature of the SiO_2–Fe_2O_3 samples (Fig. 3, Table 1). At (1388 ± 3)°C in air, the Fe_2O_3 starts to decompose to Fe_3O_4 (the first endotherm; Fig. 3a, Table 1); the decomposition is accompanied by oxygen loss and is reversible [9, 19, 20]. The incomplete dissociation of the Fe_2O_3 to Fe_3O_4 and oxygen is proven by the weight loss value: it is smaller than the values calculated from the stoichiometry (Table 1). The second endotherm, which starts at 1462°C, is due to the solidus of the FeO–Fe_2O_3 system in accordance with the FeO–Fe_2O_3 phase diagram (Fig. 5). The last endotherm (at 1473°C) is apparently due to melting of the components of the SiO_2–Fe_2O_3–Fe_3O_4 system.

Table 1. Thermal transformations in test samples

FeO_x in the sample, mol %	Iron oxide decomposition		Melting of the sample, °C		
	onset decomposition temperature, °C	iron oxide loss, wt %	onset melting	full melting	melt demixing
System SiO_2–Fe_2O_3					
94.8			1470[d]	1517[d]	
90.9			1470[d]	1505[d]	
89.6	1390[a]	2.76	1474[a]	1490[d]	
			1470[d]		
87.1	1387[a]	2.37	1473[a]	1470[d]	
			1470[d]		
85.9	1392[a]	2.67	1474[a]	1475[d]	
	1472[b]	2.31	1474[b]		
84.7	1387[a]	2.77	1472[a]	1490[d]	
	1467[b]	1.78	1470[b]		
			1470[d]		
83.4	1387[a]	2.67	1472[a]	1505[d]	
	1472[b]	2.23	1475[b]		
			1470[d]		
82.2	1389[a]	2.56	1475[a]		1539[d]
			1470[d]		
75.1			–		1530[d]
67			–		1530[d]
57.2			–		1530[d]
33.4			–		1530[d]
16.7			–		1538[d]
15.8			–		1538[d]
14.2			–	1655[d]	
12.5			–	1655[d]	
System SiO_2–Fe_3O_4					
96.2	1424[c]	1.10	1449[e]	1561[e]	
92.4			–	1548[e]	
87.5			1441[e]	1511[e]	
85.1			1445[e]	1470[e]	
81.5			1446[e]	1540[e]	
74.5			1448[e]	–	
66.7			1424[e]		1560[e]
56.0			–		1581[e]
42.8			1429[e]		1589[e]
25.0			1434[e]		1556[e]
13.8			1440[e]	1681[e]	
8.8				1681[e]	
0.8				1701[e]	

Note: [a] DTA/TG data obtained in air; [b] DTA/TG data obtained in oxygen; [c] DTA/TG data obtained in helium; [d] VPA data obtained in a high-temperature microscope; [e] VPA data obtained in Galakhov's microfurnace.

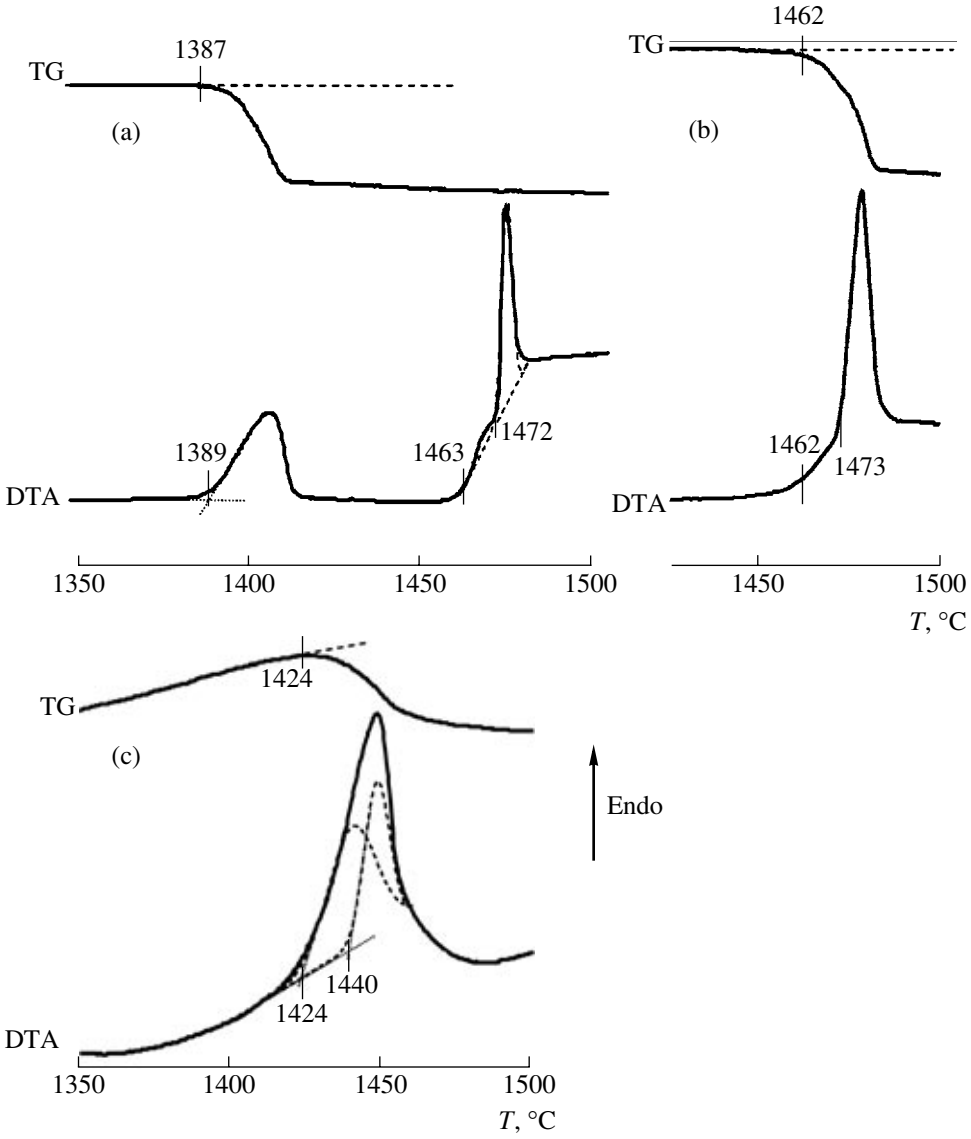

Fig. 3. (a, b) DTA and TG curves for SiO_2–Fe_2O_3 samples (a) containing 87.1 mol % FeO_x in air and (b) containing 85.9 mol % FeO_x in oxygen. (c) The same for the SiO_2–Fe_3O_4 sample containing 42.8 mol % FeO_x in helium under an overall gas pressure of $\sim 1.2 \times 10^5$ Pa.

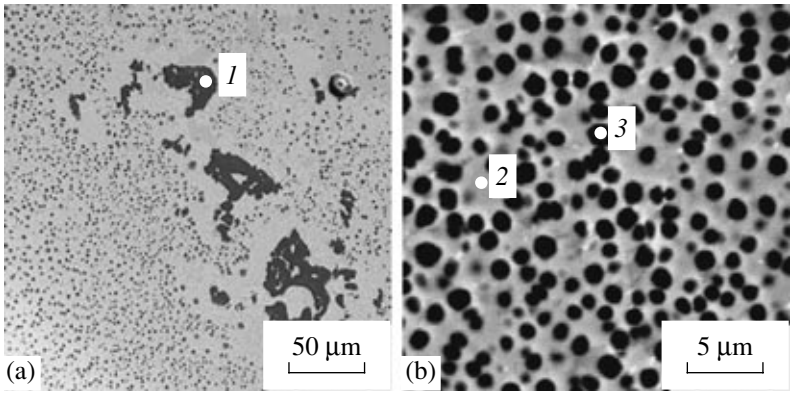

P1

Fig. 4. Micrographs of samples quenched from various temperatures after various exposures: (a) 42.8 mol % FeO_x, 1550°C (60 s); and (b) 56.0 mol % FeO_x, 1780°C (10 s). A light region is the FeO_x-based phase.

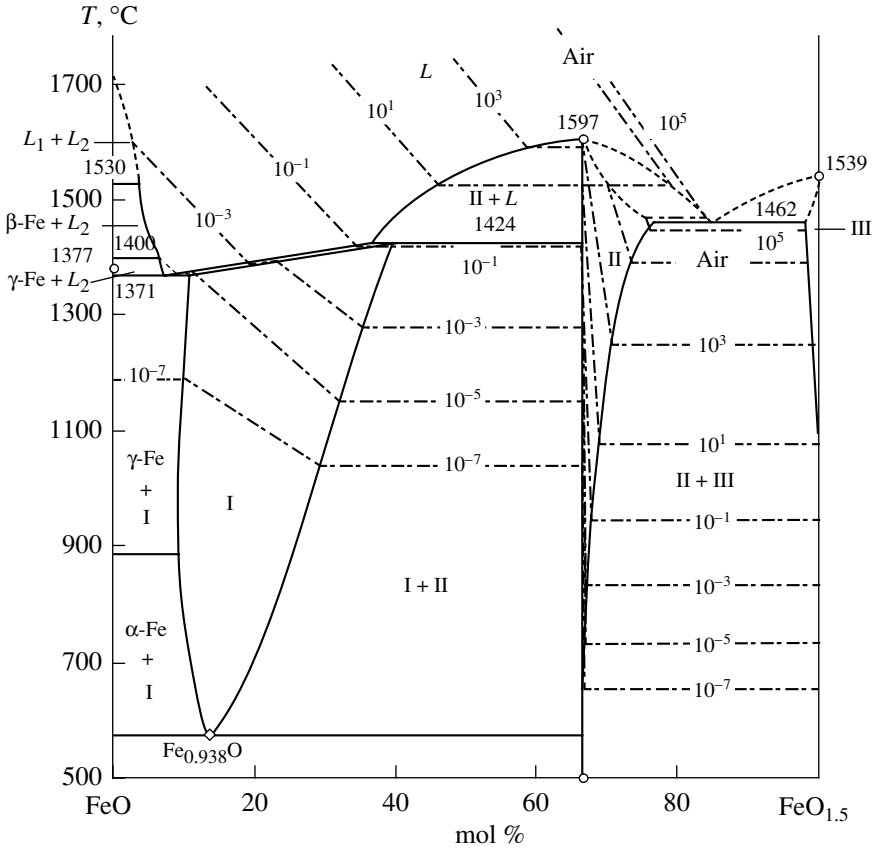

Fig. 5. FeO–Fe_2O_3 phase diagram with oxygen isobars (Pa) according to [7, 9, 10] and the refined values of the peritectic temperature in the FeO–Fe_3O_4 region and the refined eutectic temperature in the Fe_3O_4–Fe_2O_3 region.

The scheme in Fig. 6 describes the heating-induced phase and chemical transformations of the system. Cooling induces the oxidation of iron oxide (which, however, does not go to equilibrium for kinetic reasons), and Fe_2O_3 (a equilibrium phase under the specified conditions) and Fe_3O_4 (a nonequilibrium phase) coexisted in the system (Fig. 2).

Under oxygen, the dissociation $3Fe_2O_3 \longrightarrow 2Fe_3O_4 + 0.5O_2$ occurred at a higher temperature (1462°C) than in air, as we may infer from the chemical analysis results (Fig. 3b, Table 1); this higher temperature almost coincides with the onset melting temperature in the Fe_3O_4–Fe_2O_3 system (cf. Figs. 3a, 3b). Note that this temperature (1462°C) may be taken to be the solidus temperature in the Fe_3O_4–Fe_2O_3 system (Fig. 5). Thus, we somewhat refined the solidus temperature determined in [7, 9, 10] to be 1450°C (Fig. 5).

The melt immiscibility region in the SiO_2–Fe_2O_3 system was determined from the inflection point on the liquidus curve and the position of the monotectic as determined using VPA on the high-temperature microscope (Table 1).

The chemical processes occurring in the SiO_2–Fe_3O_4 samples during their heating under an argon atmosphere ($p_{O_2} < 2 \times 10^{-1}$ Pa) involved partial Fe_3O_4 decomposition with oxygen evolution at 1424°C (Fig. 3c). Another piece of evidence in favor of the occurrence of this process is the existence of the compound Fe_2SiO_4 in the samples after the DTA/TG experiments; this compound results from the reaction of FeO with SiO_2 (Fig. 2). The FeO-based phase melted simultaneously with the Fe_3O_4 decomposition (Figs. 3b, 5, 6). From the DTA (Fig. 3b) and VPA (Table 1) results, we may infer that temperature elevation to about

Table 2. EDX data for SiO_2–Fe_3O_4 samples after heat treatment

Sample			Analyzed region	
$FeO_{1.33}$ mol %	heat treatment		notation in Fig. 4	$FeO_{1.33}$, mol %
	temperature, °C	duration, s		
42.8	1550	60	1	2.0
56.2	1780	10	P1	46.5
			2	54.9
			3	35.6

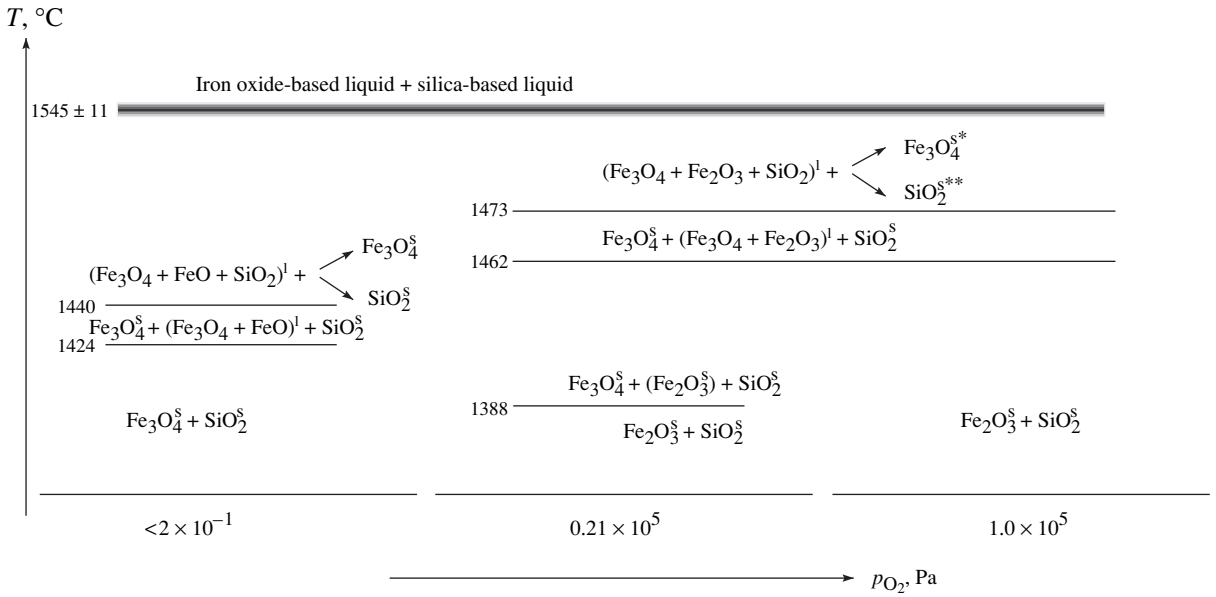

Fig. 6. Schematics of the phase and chemical transformations in the SiO_2–$Fe_2O_3(Fe_3O_4)$ system at various oxygen partial pressures. *In the region of primary crystallization of Fe_3O_4. **In the region of primary crystallization of SiO_2.

1440°C caused the components of the SiO_2–Fe_3O_4 system to melt (Fig. 6).

The VPA experiments in Galakhov's microfurnace carried out in the anneal-and-quench mode showed that the melt of the SiO_2–Fe_3O_4–(FeO) system (the minor component is parenthesized) at temperatures above 1556°C separated into two phases (an iron oxide-based phase and a silica-based phase (Fig. 4).

The average monotectic temperature for the SiO_2–$Fe_2O_3(Fe_3O_4)$ system was (1545 ± 11)°C (Table 1).

All the transformations described above are schematized in Fig. 6. An analysis of this scheme proves that the changing oxygen partial pressure over the condensed phases of the SiO_2–$Fe_2O_3(Fe_3O_4)$ systems equally affects the character and temperature of the phase and chemical transformations. The effect is above all governed by the combination of the iron oxides that exists under a given p_{O_2}. The following is noteworthy: the Fe_2O_3 and Fe_3O_4 dissociation temperatures determined in the study correlate nicely with the existing data [9, 10] and refine them only slightly. For the onset melting temperatures of the components of the SiO_2–Fe_3O_4–FeO and SiO_2–Fe_2O_3–Fe_3O_4 systems (1440 and 1473°C, respectively) and the monotectic temperature ((1545 ± 11)°C), we found substantial differences from the values that Muan cited (1665 and 1695°C, respectively) [7] with reference to Greig [3] and the values Berezhnoi cited in his handbook [13]. The differences apparently arise from the following: the high viscosities of silica-containing melts can be responsible for the overestimation of critical temperatures, which pertains to the system under consideration.

In summary, we have studied the SiO_2–$Fe_2O_3(Fe_3O_4)$ system in air, in oxygen, and under an inert atmosphere. The system experiences several phase and chemical transformations that influence the compositions of the phases involved. The compositions of the SiO_2–Fe_2O_3 samples upon heating are displaced into the SiO_2–Fe_2O_3–Fe_3O_4 ternary region both in air and in oxygen. The compositions of the SiO_2–Fe_3O_4 samples under a neutral atmosphere ($p_{O_2} \approx 2 \times 10^{-1}$ Pa) are displaced into the SiO_2–Fe_3O_4–FeO region. The melt immiscibility region is intrinsic to the SiO_2–$Fe_2O_3(Fe_3O_4)$ system at temperatures higher than (1545 ± 11)°C; the compositions of the coexisting phases are also affected by the oxygen partial pressure.

ACKNOWLEDGMENTS

The authors thank the International Science and Technology Center (the CORPHAD project) for financial support.

REFERENCES

1. V. V. Gusarov and S. A. Suvorov, Zh. Prikl. Khim. **65** (7), 1478 (1992).
2. V. V. Gusarov, A. A. Malkov, A. A. Malygin, and S. A. Suvorov, Neorg. Mater. **31** (3), 346 (1995).
3. J. W. Greig, Am. J. Sci. **14** (11), 474 (1927).
4. L. S. Darken, J. Am. Chem. Soc. **70** (6), 2046 (1948).
5. R. Schuhmann, R. G. Powell, and E. J. Michal, J. Metals, No. 9, 1097 (1953).
6. R. W. Gurry and L. S. Darken, J. Am. Chem. Soc. **72** (9), 3906 (1950).

7. A. Muan, J. Metals, No. 9, 965 (1955).
8. A. Muan and E. F. Osborn, J. Am. Ceram. Soc. **39** (4), 121 (1956).
9. L. S. Darken and R. W. Gurry, J. Am. Chem. Soc. **67** (8), 1398 (1945).
10. L. S. Darken and R. W. Gurry, J. Am. Chem. Soc. **68** (5), 798 (1946).
11. N. L. Bowen and J. F. Schairer, Am. J. Sci. **24** (139), 177 (1932).
12. N. L. Bowen, J. F. Schairer, and H. W. V. Willems, Am. J. Sci. **20** (120), 405 (1930).
13. A. S. Berezhnoi, *Multinary Oxide Systems* (Naukova Dumka, Kiev, 1970) [in Russian].
14. B. Phillips and A. Muan, J. Am. Ceram. Soc. **42** (9), 413 (1959).
15. O. B. Fabrichnaya and B. Sundman, Geochim. Cosmochim. Acta **61** (21), 4539 (1997).
16. N. A. Toropov, I. A. Bondar', A. N. Lazarev, and Yu. I. Smolin, *Silicates of Rare-Earth Elements and Their Analogues* (Nauka, Leningrad, 1971) [in Russian].
17. F. Ya. Galakhov, in *Advanced Investigation Techniques for Silicates and Civil Construction Materials* (Moscow, 1961), p. 178 [in Russian].
18. L. V. Gurvich, V. S. Iorish, D. V. Chekhovskoi, and V. S. Yungman, *IVTANTHERMO: A Thermodynamical Database and Software System for the Personal Computer. User'S Guide* (CRC Press, Boca Raton, FL, 1993).
19. J. C. Hostetter and H. S. Roberts, J. Am. Ceram. Soc. **4** (11), 931 (1921).
20. Yu. V. Levinskii, *p–T–x Diagrams for Binary Metal Systems: A Handbook* (Metallurgiya, Moscow, 1990), Vol. 1 [in Russian].
21. S. V. Beshta, E. V. Krushinov, V. I. Al'myashev, *et al.*, Zh. Neorg. Khim. (in press).